S1 Methods: model and numerical simulation

Our model for vulval induction parameterizes the dynamical process by which the two signaling pathways push the VPCs towards one of the three possible fates during the period of competence and determination (Fig. 2). We need briefly recall the experiments defining the competence period and the evidence for the geometric constructs such as fixed points that the model assumes.

The response of fate specific markers to EGF signaling begins in the late L2 larval stage ([S1]; [S3], table 1; [S15], fig. 5) and continues until shortly after the first VPC division in mid L3 (Fig. 2), when cell fate is determined and cannot be altered by the application of exogenous signals [S23]. Competence is very much a quantitative trait and not binary, and the outer limits of signal susceptibility can be explored in sensitized backgrounds. In an EGF hypomorph (where all VPCs become 3°) combined with a heat inducible source of EGF, mild heat shock at L2 lethargus gave 99% induction which fell to 53% at mid-L3 [S23]. (Stronger heat shock established that competence extended past the first division, and also that presumptive 2° cells could be converted to the 1° fate.) For EGF, anchor cell (AC) ablation provides a way of ascertaining the time after which the inductive signal is no longer necessary, which ranges from late G1 to G2/M [S5, S12]. Specification is defined as a discrete event, but happens at variable times in identical animals.

Notch response, which is necessary and sufficient for the 2° fate [S7, S21], also begins in late L2 (Fig. 2) as defined by temperature-shift experiments in a Notch gain-of-function (gf) mutant ([S7], table 8). Presumptive 3° cells will then switch to 2°, while 1° is stable (though presumptive 1° cells can be switched to 2° if Notch is applied before significant Ras induction). Determination occurs sometime after S phase, since presumptive 3° cells do not stably switch to 2° when Notch expression is limited to G1 – while Notch supplied from G2 through division does stably switch the cells [S1]. All experiments show that competence is a matter of degree, partial penetrance is the norm for most gain or loss of function experiments during the competence period and should be a feature of any quantitative model.

A strong assumption of our model is that the three fixed points and their basins of attraction exist at the beginning of competence, even though all cells begin within the 3° domain. However if one accepts that the VPCs form an equivalence group, collectively they have three allowed fates, and the common VPC network should have the three fixed points. Mathematically or computationally, multistability is frequently probed by applying a strong transient signal to the system and observing a new stable state. In biological networks there are many steps between the stimuli we can apply and the consequences we can observe. Thus the response to ligands can saturate and there are minimal intrinsic times required for changed fates to be visible (very evident for vulval induction since one is scoring division patterns). Thus directly proving that multiple fixed points exist in the VPCs at the beginning of competence is probably impossible and indirect evidence in favor of that assumption may accumulate if the various quantitative predictions of our model are born out.

S1.1 Inductive signal gradient

The gradient of inductive signal (l_1 in Eq. 4) is assumed stationary – except for AC ablation experiments, where it is set to zero after ablation. To compute the profile of the gradient, we consider as in [S10] a simple model in which EGF diffuses between discrete intercellular compartments (one per cell) indexed by $k = -2, \ldots, 2$. If n_k denotes the concentration of EGF in compartment k, the flux $\phi_{k\to k+1}$ between compartments k and $k+1$ is

$$\phi_{k\to k+1} = d(n_k - n_{k+1}) \tag{S1}$$

where d is a diffusion constant. The AC at $k = 0$ secretes a constant flux of EGF, s, which is lost at a fixed rate $r = k_d + k_b$ to degradation (k_d) and binding with receptors (k_b). The stationary profile of EGF then satisfies

$$d(n_{k+1} + n_{k-1} - 2n_k) - rn_k + s\delta_k = 0 \tag{S2}$$

where δ_k is the Kronecker delta ($\delta_k = 1$ if $k = 0$, 0 if $k \neq 0$), or

$$n_{k+1} + n_{k-1} - 2n_k - \rho n_k + c\delta_k = 0 \tag{S3}$$

where we have defined

$$\rho = r/d \tag{S4}$$
$$c = s/d \tag{S5}$$

This equation admits the solution

$$n_k = n_0 \gamma^{|k|} \tag{S6}$$

where

$$n_0 = \frac{c}{\sqrt{\rho(4+\rho)}} \tag{S7}$$
$$\gamma = \frac{2}{2+\rho+\sqrt{\rho(4+\rho)}} \tag{S8}$$

Identifying EGF signaling activity with ligand binding, i.e.

$$l_1(k) = k_b n_k \tag{S9}$$

and normalizing signal levels such that $l_1(\text{P6.p}) = 1$, we obtain our Eq. 6, $l_1 = \{\gamma^2, \gamma, 1, \gamma, \gamma^2\}$.

This simple model of EGF diffusion can be adapted to describe EGFR mutations that reduce binding by changing k_b (see S3.5).

S1.2 Simulation procedure

The Langevin equation describing VPC dynamics (Eq. 2) is solved by an Euler scheme with a time step $\Delta t = .02$:

$$\vec{r}(t_{n+1}) = \vec{r}(t_n) + \frac{\Delta t}{\tau}\left[\vec{\sigma}_1\left(\vec{f}(t_n) + \vec{m}(t_n)\right) - \vec{r}(t_n)\right] + \vec{\eta}_n \tag{S10}$$

where $\vec{\eta}_n$ is draw from a Gaussian distribution with variance $4D\Delta t$.

S1.2.1 Initial conditions

The VPCs are treated as initially equivalent, yet it is reasonable to incorporate some variability in initial conditions. A plausible choice for their distribution, requiring no additional parameters, is obtained as follows. Assuming that the dynamics prior to competence is monostable, as in Fig. 1A,D, we take our equation for the dynamics during competence (Eq. 2) and remove the term that makes it multistable, $\vec{f}(\vec{r})$, yielding

$$\frac{d\vec{r}}{dt} = \frac{1}{\tau}\left[\vec{\sigma}_1(\vec{m}_0) - \vec{r}\right] + \vec{\eta}(t) \tag{S11}$$

i.e. the cells are diffusing in a quadratic potential. The term that biases trajectories towards the default 3° fate, $\vec{m}_0$, has been retained – the initial conditions and the subsequent dynamics contribute to the bias in comparable measures. The initial state of each VPC is drawn from the resulting stationary distribution, i.e. a Gaussian distribution with variance $2D\tau$ centered at $\vec{r}_0 = \vec{\sigma}_1(\vec{m}_0)$.

S1.2.2 Fate assignment

The dynamics of VPCs is simulated from $t = 0$ to $t = 1$ with the signals active – corresponding to the competence period – then for one more unit of time without signaling to score their fates. Most cells will have ended close to a fixed point, so we can simply define fates as a function of distance to the three fixed points (d_1, d_2, d_3). For the fit to data it is desirable for model outcomes to vary continuously with parameters, so we allow fractional fates for cells at intermediate positions. We just require these to vary smoothly and recover discrete fate assignments at the fixed points; the precise definition is largely a technical matter. In practice, we assign to the three fates weights proportional to $1/d_1^2$, $1/d_2^2$, $1/d_3^2$; with this choice, the weight assigned to the 1° fate varies as $1 - O(d_1^2)$ in the vicinity of the 1° fixed point.

S2 Methods: Fit to data

Model parameters are estimated from the proportions of fates adopted by each VPC in different experimental conditions (Table S1). For this we use the methods of Bayesian inference, i.e. if D denotes the experimental data, a parameter set Θ is assigned a probability

$$P(\Theta|D) \propto P(\Theta)P(D|\Theta), \tag{S12}$$

where $P(\Theta)$ is the prior probability assigned to parameters and $P(D|\Theta)$ the likelihood of experimental observations given those parameter values. The distribution of the posterior probability $P(\Theta|D)$ over parameter space indicates how much the data constrain parameter values and the uncertainty for model predictions.

S2.1 Likelihood of experimental data

The likelihood of experimental data, $P(D|\Theta)$, is computed from the proportions of fates predicted by the model for each experiment (thus correlations between cells are ignored in the fit). Let $p^{\rm exp}_{e,c,f}$ and $p^{\rm num}_{e,c,f}(\Theta)$ denote the fractions of animals in which cell c adopts fate f in experiment e and the corresponding simulation, respectively. The likelihood of the data is approximated as

$$P(D|\Theta) \approx e^{-\frac{\chi(\Theta)^2}{2}} \tag{S13}$$

where

$$\chi^2(\Theta) = N \sum_{e,c,f} \left(p^{\rm exp}_{e,c,f} - p^{\rm num}_{e,c,f}(\Theta) \right)^2 \tag{S14}$$

where N is a typical number of animals sampled experimentally, taken to be $N = 64$. Several approximations are made here. We have assigned the same expected variance N to each data point, while it would be smaller for infrequent outcomes if sampling errors were the only source of fluctuations. But there can be other sources of uncertainty, e.g. in the scoring of ambiguous lineages observed experimentally. In addition, different sample sizes are available for different experiments, but we prefer not to give more weight to any particular phenotype. Numerical frequencies are also computed from finite samples, and greater sample sizes could limit their contribution to uncertainty. Experiments were made with 64 and 256 samples, and little difference was observed, so the smaller value was used to limit computation time.

An exception to the above estimation of likelihood is made for SynMuv (*lin-15*) mutants, in which EGF is ectopically expressed from the hypodermis surrounding VPCs [S4]. Any VPC in isolation would then adopt the 1° fate, but because of lateral signaling, alternating patterns of 1°s and 2°s are obtained, in which adjacent 1°s are infrequent [S19]. This phenotype, which is observed whether or not an AC is present, cannot

be captured by separate fate probabilities for the different cells. In the absence of detailed pattern statistics, it is incorporated in our χ^2 as a term

$$N\left((p_3^{\text{num}})^2 + (p_{11}^{\text{num}})^2 + (p_2^{\text{num}} - 1/2)^2 H(p_2^{\text{num}} - 1/2)\right) \tag{S15}$$

where H is Heavyside's function, p_2^{num} (resp. p_3^{num}) is the numerical frequency of the 2° (resp. 3°) fate averaged over cells, and p_{11}^{num} is the frequency of adjacent 1° cells. As described in S1.2.2, each cell in a simulation run contributes fractional weights to each fate, e.g. s_c^1 is the weight of fate 1° for cell c. The proportion of adjacent 1°s for a run (whose average over runs is p_{11}^{num}) is defined as

$$\frac{1}{4}\sum_{c=1}^{4} s_c^1 s_{c+1}^1 \tag{S16}$$

The different terms in Eq. S15 penalize 3° fates, adjacent 1° fates, and 2° fates in excess of 50% (this excludes patterns made of all 2°s, which are a trivial solution of the other constraints; alternating patterns of 1°s and 2°s are observed experimentally [S19]).

S2.2 Priors

Table S2 lists the priors for the different parameters. Some parameters are naturally bounded (e.g. γ and the relative level of EGF in a hypomorph are between 0 and 1) and are assigned flat priors. The $\vec{m}_i$, for which we want to favor small values – the pathway sensitivities should not be arbitrarily large – are assigned Gaussian priors,

$$P(\vec{m}_i) \propto e^{-\frac{\vec{m}_i^2}{2\sigma_i^2}} \tag{S17}$$

Other (positive) parameters are not bounded but we do not have the same strong subjective bias for small values (the level of EGF when overexpressed is an example), and for these we use exponential priors,

$$P(\theta_i) \propto e^{-\frac{\theta_i}{\beta_i}} \tag{S18}$$

where β_i defines a reasonable scale for parameter θ_i, e.g. for EGF overexpression the value has to be significantly greater than 1 and we set $\beta = 4$. Most parameters we find are constrained by the data so the priors have little influence. This is not the case for the signal response strengths m_i, for which there is greater uncertainty.

S2.3 Exploration of parameter space

The logarithm of the posterior probability can be expressed as a sum of squares, provided we rewrite exponential priors (Eq. S18) as

$$e^{-\frac{\theta_i}{\beta_i}} = e^{-\sqrt{\frac{\theta_i}{\beta_i}}^2} \tag{S19}$$

This allows local optima to be computed efficiently using the Levenberg-Marquardt algorithm [S16]. For this we need the numerical fate frequencies to be smooth functions of parameters so we freeze the noise: a set of realizations of the noise $\{\vec{\eta}_n\}$ (Eq. S10) is tabulated for each cell and used throughout. The local optimum to which the algorithm converges depends on the noise samples, but by construction, these variations remain within parameter uncertainty. When fitting the data in Table S1, we can clearly identify a unique global optimum that is well separated from other local optima.

To ascertain indeterminacy in parameter values (which defines our confidence in model predictions), we explore the vicinity of the global optimum using a Markov chain Monte Carlo algorithm. In each trial move,

we step both model parameters and the tabulated noise samples (replacing a small, randomly selected fraction), which eliminates any bias from frozen noise. In parameter space, the trial steps are chosen adaptively, according to the covariance matrix of past steps in the chain [S8]. This allows efficient exploration even if the distribution is anisotropic (i.e. some parameter combinations are better constrained than others).

The means and standard deviations of parameter values for our main fit are shown in Table S3. Most parameters are individually constrained. In the following section we relate these constraints to individual experiments; most informative are experiments in which a cell exhibits variable fates, which places the outcomes over a boundary between two basins of attraction.

S2.4 Constraints on parameters

Repeating the fit with different subsets of experimental data indicates how individual phenotypes constrain parameter values, and we can understand these constraints by examining the trajectories of cells in the model. Experiments that give reproducible outcomes (e.g. WT outcomes) yield inequalities on parameters (the average outcome for each cell is well into a fate domain), while experiments with variable outcomes place the outcome for at least one cell on a boundary and yield approximate equalities.

S2.4.1 Single cell response

To understand how parameters are tied to phenotypes, it is useful to first consider the response of a single cell to variable levels of inductive or lateral signal (in the absence of autocrine signaling). The predicted sigmoidal response curves are similar to that of a one-dimensional, two-state switch (Figs. S1 and S2). An average induction of a half is obtained at a level $l_1^{50\%}$ (resp. $l_2^{50\%}$) such that the initial conditions flow into the saddle between the 3° and 1° (resp. 3° and 2°) fates, as in Fig. 4C,E. The equations of the model (Eqs. 1-4) and our choice of initial conditions (cf. S1.2.1) imply that $l_i^{50\%} \approx 2m_0/m_i$, which is confirmed by the scatter plots in Figs. S1b and S2b. Uncertainty in the values of the m_i makes the induction thresholds (Figs. S1a and Fig. S2a) ambiguous. When signal levels are normalized to the threshold level for each parameter set, the induction curves collapse onto a common shape (Figs. S1c and S2c). The width of the induction curve is a direct measure of the noise parameter D in the model and the fit of that parameter to the ablation data discussed below then predicts that a two-fold increase in the level of either signal is sufficient to go from almost no to almost full induction.

S2.4.2 Reduced Notch signaling

Notch null mutants have two ACs (Notch signaling is also involved in the specification of the AC), and P5/7.p are then induced to the 1° fate in most animals [S7]; assuming two ACs yield twice as much EGF, this implies $2\gamma > l_1^{50\%}$ (γ is the level seen by P5/7.p in WT).

On the other hand, several observations suggest that the WT level of EGF received by P5/7.p is insufficient to induce the 1° fate, or $\gamma < l_1^{50\%}$. P7.p can adopt the 3° fate in animals bearing a weak hypomorphic allele, *lin12(n676n930)*, that have a single AC [S22]. A similar outcome is obtained in mosaic animals in which P6.p lacks EGF receptors and does not adopt the 1° fate [S18]. In animals lacking OSM-11, an activator of Notch signaling, P5/7.p most often fail to express reporters of either the 1° or the 2° fate [S14]. Finally, P5/7.p adopt the 3° fate (as defined by reporter expression and cell morphology) when lateral signaling is impaired by preventing internalization of Notch receptors in P6.p [S17].

Together, these inequalities on γ yield $\gamma \lessapprox l_1^{50\%}$ (or $\gamma \lessapprox 2m_0/m_1$; Fig. S4). This explains our observation that in wild-type EGF keeps P5/7.p balanced between the 3° and 1° fates before the onset of lateral signaling from P6.p (Fig. 8).

Note that in the absence of more quantitative data, the above experimental outcomes are idealized for the purpose of the fit as the phenotypes 31113 and 33133 (Table S1, lines 5 and 6). These experiments just bound γ from above and below, so the approximation should be of little consequence.

S2.4.3 EGF overexpression

EGF overexpression from the anchor cell is parameterized by increasing inductive signaling by a factor l_1^{over}. Table S1, line 7 gives the outcomes in experiments where an average of about 4 cells are induced [S10], and Fig. 6 shows the corresponding trajectories. P5/7.p yield mixed 1°/2° fates, implying a balance between the enhanced inductive signal from the AC (γl_1^{over}) and the lateral signal from P6.p (≈ 1), or $\gamma l_1^{\text{over}} m_1 \approx m_2$. P4/8.p yield a fraction of all three fates, so the level of inductive signal they receive must be close to threshold, $\gamma^2 l_1^{\text{over}} \approx l_1^{50\%}$. Combining these relations with $\gamma \lessapprox l_1^{50\%}$ (cf. S2.4.2) yields $l_1^{\text{over}} \gtrapprox 1/\gamma$ and $m_1 \lessapprox m_2$ (Fig. S3).

S2.4.4 AC ablation

AC ablation experiments (Table S1, lines 9-14) are modeled by shutting off inductive signaling. Figure 7A shows the resulting trajectories, with an enhanced scatter of outcomes relative to WT (cf. Fig. 5A). Ablations probe the time course of induction: the progressive transition from no induction to a WT pattern (Fig. S5) determines both τ and D in Eqs. 2,5 in the dynamics. The mixed 1°/2° fates adopted by P6.p at intermediate times rely on the diffusing Delta fraction and autocrine signaling to drive cells into the 2° domain, constraining the value of the autocrine-to-paracrine ratio α (Eq. 9). In the absence of precise timing information, the developmental stages that define ablation times [S15] were mapped to regularly spaced time points in the interval [.2, .8] (crosses in Fig. 5B). Note however that the mixed 1°/2° fates are essentially determined by the geometry of the flow, rather than precise timing (Fig. S9). Thus the actual times we chose to represent the data will correctly represent the trends in the ablations (and what ever time is required for EGF protein to decay) but may not be linearly proportional to physical time. However once an ablation is fit for WT, we can predict its effect in any genetic background without reconsidering the times.

S2.4.5 Threshold for lateral signaling

The timing of P5/7.p induction in AC ablation experiments constrains the timing of lateral signaling, i.e. the position of the signaling threshold n_0 in the expression for L_2 in Eq. 7. In the EGF overexpression experiment, P5/7.p are on the boundary between 2° and 1° and partially induce P4/8.p to a 2° fate, which imposes a constraint on the orientation $\angle\vec{n}_1$ of the threshold.

S3 Model predictions

S3.1 Intrinsic/extrinsic noise

Correlations between cell fates in model and experiments are shown in Table S5, which compares observed pattern frequencies for P5-7.p to the frequencies expected in the absence of correlations. In the EGF hypomorph *lin-3(e1417)* (Table S4), P5/7.p are almost never induced when P6.p is not, an obvious source of correlations. As a more stringent test, we consider separately animals in which P6.p adopts the 1° fate, of which there is a fraction $P(\text{P6.p} \to 1°)$. We estimate the conditional probabilities of the three fates in P5/7.p, e.g. $P(\text{P5.p} \to 2°|\text{P6.p} \to 1°)$, as the fractions of those animals in which cells adopt a given fate. Then we can compute the expected frequency of any pattern where P6.p adopts the 1° fate in the absence

of correlations between P5/7.p, e.g.

$$P(2^\circ 1^\circ 3^\circ) = P(\text{P6.p} \to 1^\circ) P(\text{P5.p} \to 2^\circ | \text{P6.p} \to 1^\circ) P(\text{P7.p} \to 3^\circ | \text{P6.p} \to 1^\circ) \tag{S20}$$

Because model predictions for individual cell fate probabilities never coincide exactly with experiment – e.g. there can be slight experimental asymmetries between P5.p and P7.p, which are absent in the model – these randomized pattern frequencies are computed separately for model and experiment.

For the EGF hypomorph, we used a separate fit of model parameters where the hypomorph phenotype in Table S4 was added to the training data. Although we can predict the induction of P5/7.p to within a reasonable error from our main fit (Fig. S7), fitting it explicitly makes for a cleaner comparison of correlations in model and experiment. Our results show that, even among those animals in which P6.p is induced to the 1° fate, the variability of its developmental trajectory induces correlated fluctuations in the fates of its neighbors, P5/7.p. This also occurs, although to a lesser extent, following AC ablation at an intermediate time. In contrast, the correlations disappear when EGF is overexpressed from the anchor cell and P6.p is robustly induced.

S3.2 Marginal crosses

In addition to epistasis between marginal EGF and Notch hypomorphs, described in the main text (Fig. 8), we have systematically explored other combinations of marginal mutations. Marginal overexpression of EGF from the anchor cell displaces the outcomes for presumptive 2° cells (P5/7.p) closer to the 1° fate (Fig. S11a). If this is combined with a marginal reduction in Notch activity, the increased EGF signaling overrides lateral signaling from P6.p and P5/7.p are converted to the 1° fate with high probability (Fig. S11b,c). Gain-of-function Notch mutations result in constitutive activation of the pathway, and are treated in the model as a uniform additive term in l_2 (cf. Eq. 4). Strong mutations result in loss of the AC and the adoption of the 2° fate by all VPCs; weaker mutations yield less penetrant defects. In the model, a marginal additive increase in Notch activity (EGF activity being normal) displaces presumptive 3° cells (P4/8.p) near the 2° fate (while P5-7.p are unaffected; Fig. S12a). When this is crossed with a marginal EGF hypomorph, we predict a WT outcome (Fig. S12b). On the other hand, when it is crossed with a marginal increase in EGF activity (multiplicative as previously), P5/7.p come closer the 1° fate early in their trajectory and produce more lateral signal, driving P4/8.p into the 2° fate (Fig. S12c,d). Thus we predict the unexpected result that increased EGF signaling enhances the induction of 2° fates – an effect of intercellular coupling.

S3.3 Epistasis from saddle flows

Non-intuitive epistatic effects can be induced by the flow near a saddle point, as observed when weak EGF signaling is introduced in a background with weak constitutive Notch activity (Fig. 9). The same phenomenon occurs, with the roles of Notch and EGF interchanged, when we simulate the cross of the EGF hypomorph *lin-3(e1417)* (Table S4; 58% induction of P6.p) with a marginal Notch hypomorph (Fig. S13). P6.p in the EGF hypomorph flows to the saddle between the 3° and 1° fates (Fig. S9c). With our canonical vertical direction of the vector $\vec{m}_2$ representing Notch response (Eq. 4), reduced Notch activity does not affect the induction of P6.p to the 1° fate since it displaces the initial conditions along the flow into the saddle. This can come as a surprise if Notch and EGF are seen as antagonistic, and if the direction of $\vec{m}_2$ is slightly altered (30° towards the 1° fate), reduced Notch can even *decrease* P6.p induction to the 1° fate (Fig. S13d).

S3.4 Putative epistasis between Notch and EGF pathways

Sensitized backgrounds were employed to study the mutual inhibition between EGF and Notch signaling, and since our model combines the pathways without interaction, it is important to consider this data. Berset et

al. [S2] present biochemical data implicating the MAPK phosphatase LIP-1 in a pathway that downregulates EGF signaling in P5/7.p in response to Notch signaling. However a *lip-1(lf)* mutation has no phenotype, so their genetic strategy was to cross this allele into a background that up regulated EGF e.g. *lin-15(rf)* and observe epistasis. To replicate their genetic experiment, we model *lip-1(lf)* as a multiplicative increase in the EGF scale l_1 in every cell that is marginal, i.e., a slightly larger value as a phenotype. The *lin-15(rf)* allele was part of our fitting set (though the assay was different). We can then predict the correct percent induction of 1° fates in P5/7.p (Table S6). So we explain the epistasis in this genetic cross, not as pathway interaction since we have no such term, but rather as a consequence of the nonlinear projection onto cell fates.

S3.5 Shape of the EGF gradient

The shape of the gradient of EGF, described in WT by $l_1(\text{P6.p}) = 1$ and the decay factor γ, may change in different backgrounds. For instance, Hajnal et al. [S9] suggest that EGFR sequesters ligand and prevents ectopic vulval induction, based on the observation that EGFR(rf) *enhances* induction in a sensitized background (silent mutation in *gap-1*, a negative regulator of inductive signaling). A mutation in EGFR that reduces EGF binding would be described by reducing the rate k_b (cf. S1.1). Although this reduces the rate of signaling for a given concentration of extracellular EGF, both the maximum level and range of EGF increase (Eqs. S7 and S8), so that signaling in distal cells can *increase*. When we start from the rather steep gradient we predict in WT, it is easy to increase the spreading of EGF so that its level is increased by 3× on P4/8.p. We then find enhanced induction in sensitized backgrounds, such as doubling l_1 (with no phenotype in WT), where P4/8.p most often adopt a 1° fate and the dominant pattern is 12121.

S3.6 Isolated cells

Isolated 2° cells are found experimentally when all but one VPC are ablated [S10, S11, S20]. One model for lateral signaling, suggested by the EGF hypomorph phenotype (P6.p adopts 3°/1° fates), assumes that secreted Delta ligands are removed by degradation and there is no competition for their uptake. But then isolated cells are no different than P6.p in the EGF hypomorph (since P5/7.p do not express Delta), and there is no way to obtain isolated 2°s (Fig. S14a). An alternative model for the fate of diffusing Delta is that cells compete for its uptake. Then an isolated cell will receive a stronger signal than one with two neighbors, e.g. 3× if diffusing Delta is shared evenly between a secreting cell and its neighbors. We find increases in Notch signaling of this order can land an isolated cell at the meeting point between the 3 domains (Fig. S14b), yielding a mixture of all fates as in experiments [S10]. (This prediction requires us to adjust the EGF level since cells move an indeterminate amount following ablation). Outcomes in the model are clustered near the 1°/2° boundary and we predict a high occurrence of hybrid fates, which is indeed observed experimentally (cf. S3.9 and Table S7).

S3.7 Anchor cell ablation in mutants

We can predict the outcome of AC ablation experiments in mutants. In WT, P6.p adopts approximately equal proportions of 1° and 2° fates in a range of ablation times (Fig. S5), and a natural expectation would be that mutations affecting EGF/Notch signaling shift this balance [S5]. Strikingly, we find that the relative proportion of 1° and 2° fates varies according to Notch level, but variations in EGF only affect the timing of induction: a later ablation in a hypomorph yields the same induction as an earlier ablation in WT, but the proportions of 1° and 2° are the same (Fig. S10). Ablation experiments in mutants have been reported in [S5], but most of the mutations considered do not simply up or down-regulate either of the pathways, complicating the interpretation of their effect.

S3.8 Temperature steps

In WT, the trajectory of induced VPCs takes them directly from the basin of attraction of the default 3° fate to that of their eventual fate (Fig. 5A). However, under a uniform level of inductive signal that yields the pattern 12121 (e.g. in an AC-ablated *lin-15(ts)* mutant at a suitable temperature), the trajectory for P5/7.p passes through the 1° domain on its way to the 2° fate (Fig. S15b). The intermediate 1° fate would be revealed by a temperature shift experiment that delayed induction (Fig. S15), thus yielding the surprising result that less EGF signaling can generate more 1° fated cells.

S3.9 Hybrid fates

Our model in its simplest form treats VPCs as indivisible – a VPC has a single state and yields a single fate – and the data we fit to is commonly summarized in this way. However experiments sometimes show VPC daughters assume different fates as defined by their terminal division patterns (e.g. [S7, S20]). Qualitatively we would predict more hybrid fates in a background when most VPCs fall on a boundary (e.g. P5/7.p in Fig. 6), rather than being spread out normal to a boundary (e.g. P5/7.p in Fig. 7A and P6.p in Fig. 7B). However we can be quantitative by including cell division in our model and scoring separately the fates of daughters. For simplicity we divide cells at the end of competence (actually competence extends shortly after VPC division, cf. Fig. 2), and each daughter inherits the state of its mother. Then, following the same procedure as for VPCs (cf. S1.2.2), we compute the trajectory of each daughter for one more unit of time without signaling, after which its location defines its fate. Because of noise, when a VPC is close to the boundary between two basins of attraction at the end of competence, its daughters can take divergent paths and yield different fates. The results are shown in Table S7, along with the corresponding experimental data. The frequencies of hybrid fates in the model behave according to our expectations, i.e. there are more hybrid fates when outcomes are clustered near a boundary. In that case (e.g. for isolated cells), there is reasonable quantitative agreement with experimentally observed frequencies. On the other hand, when outcomes are spread across a boundary, we predict too few hybrid fates, thus other factors not included in this simple treatment may contribute to their occurrence, e.g. asymmetry in the states of daughters upon division, signaling from the anchor cell and between daughter cells between division and the end of competence, etc. These effects could be incorporated in a more detailed description of daughter cells.

References

[S1] V Ambros. Cell cycle-dependent sequencing of cell fate decisions in *Caenorhabditis elegans* vulva precursor cells. *Development*, 126:1947–56, 1999.

[S2] T Berset, E F Hoier, G Battu, S Canevascini, and A Hajnal. Notch inhibition of RAS signaling through MAP kinase phosphatase LIP-1 during *C. elegans* vulval development. *Science*, 291:1055–8, 2001.

[S3] R D Burdine, C S Branda, and M J Stern. EGL-17(FGF) expression coordinates the attraction of the migrating sex myoblasts with vulval induction in *C. elegans*. *Development*, 125:1083–93, 1998.

[S4] M Cui, J Chen, T R Myers, B J Hwang, P W Sternberg, I Greenwald, and M Han. SynMuv genes redundantly inhibit *lin-3/EGF* expression to prevent inappropriate vulval induction in *C. elegans*. *Dev Cell*, 10:667–72, 2006.

[S5] M-A Félix. Cryptic quantitative evolution of the vulva intercellular signaling network in *Caenorhabditis*. *Curr Biol*, 17:103–14, 2007.

[S6] E L Ferguson and H R Horvitz. Identification and characterization of 22 genes that affect the vulval cell lineages of the nematode *Caenorhabditis elegans*. *Genetics*, 110:17–72, 1985.

[S7] I Greenwald, P W Sternberg, and H R Horvitz. The *lin-12* locus specifies cell fates in *Caenorhabditis elegans*. *Cell*, 34:435–44, 1983.

[S8] H Haario, E Saksman, and J Tamminen. An adaptive Metropolis algorithm. *Bernoulli*, 7:223–242, 2001.

[S9] A Hajnal, C W Whitfield, and S K Kim. Inhibition of *Caenorhabditis elegans* vulval induction by *gap-1* and by *let-23* receptor tyrosine kinase. *Genes & Development*, 11:2715–28, 1997.

[S10] E Hoyos, K Kim, J Milloz, M Barkoulas, J-B Pénigault, E Munro, and M-A Félix. Quantitative variation in autocrine signaling and pathway crosstalk in the *Caenorhabditis* vulval network. *Curr Biol*, 21:527–538, 2011.

[S11] W S Katz, R J Hill, T R Clandinin, and P W Sternberg. Different levels of the *C. elegans* growth factor LIN-3 promote distinct vulval precursor fates. *Cell*, 82:297–307, 1995.

[S12] J Kimble. Alterations in cell lineage following laser ablation of cells in the somatic gonad of *Caenorhabditis elegans*. *Dev Biol*, 87:286–300, 1981.

[S13] M Koga and Y Ohshima. Mosaic analysis of the *let-23* gene function in vulval induction of *Caenorhabditis elegans*. *Development*, 121:2655–66, 1995.

[S14] H Komatsu, M Y Chao, J Larkins-Ford, M E Corkins, G A Somers, T Tucey, H M Dionne, J Q White, K Wani, M Boxem, and A C Hart. OSM-11 facilitates LIN-12 Notch signaling during *Caenorhabditis elegans* vulval development. *PLoS Biol*, 6:e196, 2008.

[S15] J Milloz, F Duveau, I Nuez, and M-A Félix. Intraspecific evolution of the intercellular signaling network underlying a robust developmental system. *Genes & Development*, 22:3064–3075, 2008.

[S16] W H Press, S A Teukolsky, W T Vetterling, and B P Flannery. *Numerical Recipes*. Cambridge University Press, third edition, 2007.

[S17] D D Shaye and I Greenwald. Endocytosis-mediated downregulation of LIN-12/Notch upon Ras activation in *Caenorhabditis elegans*. *Nature*, 420:686–90, 2002.

[S18] J S Simske and S K Kim. Sequential signalling during *Caenorhabditis elegans* vulval induction. *Nature*, 375:142–6, 1995.

[S19] P W Sternberg. Lateral inhibition during vulval induction in *Caenorhabditis elegans*. *Nature*, 335:551–4, 1988.

[S20] P W Sternberg and H R Horvitz. Pattern formation during vulval development in *C. elegans*. *Cell*, 44:761–72, 1986.

[S21] P W Sternberg and H R Horvitz. The combined action of two intercellular signaling pathways specifies three cell fates during vulval induction in *C. elegans*. *Cell*, 58:679–93, 1989.

[S22] M Sundaram and I Greenwald. Genetic and phenotypic studies of hypomorphic *lin-12* mutants in *Caenorhabditis elegans*. *Genetics*, 135:755–63, 1993.

[S23] M Wang and P W Sternberg. Competence and commitment of *Caenorhabditis elegans* vulval precursor cells. *Dev Biol*, 212:12–24, 1999.

Table S1: Experimental data used to fit model parameters

	Experiment	VPC fates (fate or % 1°,2°,3°)					References
		P4.p	P5.p	P6.p	P7.p	P8.p	
	Wild-type outcomes under reduced signaling						
(1)	Wild type	3°	2°	1°	2°	3°	
(2)	*let-23* mosaic (no EGF receptors in P5/7.p)			wild type			[S13, S18]
(3)	Half dose of *lin-3* (EGF ligand)			wild type			[S6]
(4)	Half dose of *lin-12* (Notch receptor)			wild type			[S7]
	Phenotypes under reduced Notch/excess EGF						
(5)	Notch null, 2×WT EGF (2 ACs)	3°	1°	1°	1°	3°	[S7]
(6)	No Notch signaling, WT EGF	3°	3°	1°	3°	3°	[S14, S17, S22]
(7)	EGF overexpression	24,54,21	54,46,0	96,4,0	37,63,0	12,38,50	[S10]
(8)	*lin-15* (ectopic EGF) (with or without AC)			alternating patterns of 1°/2°			[S19]
	Phenotypes following anchor cell ablation						[S15]
(9)	L2 lethargus ($t = .2$)	–	3°	3°	3°	–	
(10)	early L3 ($t = .32$)	–	3,22,75	18,18,65	0,20,80	–	
(11)	DU divided ($t = .44$)	–	0,59,41	31,38,31	0,54,46	–	
(12)	VU divided ($t = .56$)	–	0,95,5	53,48,0	8,85,8	–	
(13)	3° divided ($t = .68$)	–	3,98,0	65,35,0	0,100,0	–	
(14)	2-cell stage ($t = .8$)	–	1,99,0	93,7,0	1,99,0	–	

The experiments are categorized as in the summary Table 1, and the outcome or proportions of different fates are given for each, along with the corresponding reference in the literature (dashes denote data not reported). Quantitative phenotypes were scored from published cell lineages as described in [S10]. Ambiguous fates, where two daughters of a VPC exhibit lineages characteristic of different fates, contribute a weight of a half to each.

Table S2: Model priors

Parameter	Prior
m_0	$\sigma = 1$
m_1	$\sigma = 4$
m_2	$\sigma = 4$
$\frac{1}{\tau}$	$\beta = 4$
$\sqrt{4D}$	$[.05, .5]$
γ	$[0, 1]$
α	$\beta = 1$
n_0	$\sigma = 4$
$\angle\vec{n}_1$	$[-180°, 180°]$
l_1^{over}	$\beta = 4$
l_1^{lin-15}	$\beta = 1$

For bounded parameters, we indicate their allowed range; for Gaussian priors, the standard deviation σ (Eq. S17); for exponential priors, the scale β (Eq. S18). The noise level is internally represented as $\sqrt{4D}$, the length scale of diffusion in one unit of time. We also indicate the priors for the level of l_1 estimated for the EGF overexpression experiment and *lin-15* mutant (Table S1, lines 7 and 8).

Table S3: Parameter values from our main fit

Parameter	mean±SD
m_0	0.39±0.03
m_1	4.60±0.98
m_2	5.97±1.07
$\frac{1}{\tau}$	2.18±0.30
$\sqrt{4D}$	0.16±0.04
γ	0.16±0.03
α	1.14±0.17
n_0	-1.23±0.10
$\angle\vec{n}_1$	-48.28±3.34
l_1^{over}	7.39±1.36
l_1^{lin-15}	0.55±0.25

The mean and standard deviation are indicated for each parameter, as computed from Monte Carlo sampling of parameter space. Also shown are the values of l_1 estimated for the EGF overexpression experiment and *lin-15* mutant (Table S1, lines 7 and 8). Most values are constrained to within 20%.

Table S4: Phenotype of the EGF hypmorph *lin-3(e1417)*

VPC fates (% 1°,2°,3°)				
P4.p	P5.p	P6.p	P7.p	P8.p
0,0,100	2,14,84	57,1,42	0,14,86	0,0,100

Data from the laboratory of Marie-Anne Félix ($n = 150$ animals).

Table S5: Intrinsic/extrinsic fluctuations

EGF overexpression				
111	27	26	19	17
112	21	22	29	31
211	22	23	16	17
212	21	20	32	31

EGF hypomorph				
212	4.3	2.5	6.9	2.9
213	8.6	11	5.8	10
312	7.7	10	5.6	10
313	43	41	38	34

AC ablation				
2V2	38	33	42	32
2V3	11	16	8.3	18
3V2	10	15	1.3	11
3V3	12	6.9	16	6.2

Frequencies of patterns adopted by P5-7.p in three conditions: EGF overexpression (Table S1, line 7; [S10]), an EGF hypomorph (*lin-3(e1417)*, Table S4), and AC ablation at an intermediate time (Table S1, line 11; [S15]). For each pattern (111, 112, etc.) we indicate its frequency (%) in the model (in black; $n = 1024$ runs) and in experiments (in red). For both model and experiments, we show in blue the pattern frequencies expected if the fates of P5/7.p were uncorrelated, as explained in the text. For the EGF overexpression and hypomorph, we show only those patterns in which P6.p adopts the 1° fate (representing 57% of animals for the hypomorph; cf. Table S4). For AC ablation, P6.p when induced can adopt either the 1° or 2° fate, and the two vulval fates are pooled together (denoted as 'V'). P5/7.p appear uncorrelated in the overexpression experiment: frequencies in model (black) and experiments (red) agree with the expectations (blue). On the other hand, in the EGF hypomorph, the fates of P5/7.p are strongly correlated (e.g. the pattern 212 where both P5/7.p are induced is over-represented). Similar correlations – albeit weaker – are obtained following AC ablation at the DU divided stage ($t = .32$ in the model).

Table S6: Interaction between *lin-15* and *lip-1*

Mutant	% 1° fate				
	P4.p	P5.p	P6.p	P7.p	P8.p
lin-15(rf)	97 ± 4	1 ± 1	99 ± 1	1 ± 1	97 ± 5
	71	0	100	4	79
lip-1(lf)	0 ± 1	1 ± 1	99 ± 1	1 ± 1	1 ± 1
	0	0	100	0	0
lin-15;lip-1	99 ± 1	64 ± 35	99 ± 1	67 ± 33	99 ± 1
	60	40	100	30	87
"*lip-1*×*lin-15*"	98 ± 2	2 ± 3	99 ± 1	2 ± 4	98 ± 2

Predicted induction of 1° fates in the double mutant *lin-15(rf);lip-1(lf)*. Corresponding experimental data are shown in red (1° fates scored by the expression of EGL-17 [S2]). *lin-15(rf)* (ectopic EGF, modeled as additive uniform $\delta l_1 \approx .5$) is part of the fitting data (Table S1, line 8). *lip-1* is fit as a marginal fold-increase, $c \approx 4$, in EGF. Note that *lin-15* is upstream of *lip-1* so the cross is represented as $c \times (l_1 + \delta l_1)$. The reverse order would have much less effect ($(c \times l_1) + \delta l_1$; shown as "*lip-1*×*lin-15*" in the table).

Table S7: Daughter cell fates

Experiment	P4.p			P5.p			P6.p			P7.p			P8.p		
EGF hypomorph	3°	100	100	3°	90	76	1°	57	44	3°	88	79	3°	100	100
				2°	8	4	3°	39	30	2°	10	6			
				2°/3°	1	17	1°/3°	3	24	2°/3°	2	15			
				1°/3°	1	3	1°/2°	1	2	1°/3°	1	0			
EGF overexpression	2°	58	26	1°	46	40	1°	100	92	1°	46	19	2°	58	14
	3°	28	26	2°	36	32	1°/2°	0	8	2°	34	44	3°	30	48
	1	10	0	1°/2°	14	28				1°/2°	15	37	1°	10	0
	2°/3°	2	4	1°/3°	2	0				1°/3°	3	0	2°/3°	1	17
	1°/3°	1	0	2°/3°	2	0				2°/3°	2	0	1°/3°	1	3
	1°/2°	1	44										1°/2°	1	17
Isolated cell	1°	41	34												
	2°	24	19												
	1°/2°	18	32												
	3°	8	11												
	1°/3°	5	4												
	2°/3°	3	0												

The frequencies of hybrid fates predicted by a modified model that treats VPC daughters separately are shown in black, with the corresponding experimental data in red. For each pair of fates, the two possible hybrids (e.g. 1°/2° and 2°/1°) are pooled together; infrequent outcomes (< 1%) are not shown. For the EGF hypomorph, experimental data are for the allele *lin-3(e1417)* (Table S4) and parameter values for the model were taken from a fit with that mutant added to the training data. The EGF overexpression experiment is that included in our data set (Table S1, line 7; [S10]). Experimental data for isolated cells were obtained following laser ablation of all VPCs but P4.p [S10] and the outcome was modeled as described in Fig. S14b. Numerical results are consistent with our expectation that more hybrid fates should be obtained when the outcomes for a VPC are clustered near a boundary (e.g. P5/7.p when EGF is overexpressed) than when they are spread across the boundary (e.g. P6.p in the EGF hypomorph). Our predictions for the cases with frequent hybrid fates are in reasonable quantitative agreement with experiments (e.g. for isolated cells), but we otherwise understimate their frequency, suggesting other factors contribute to their occurrence.

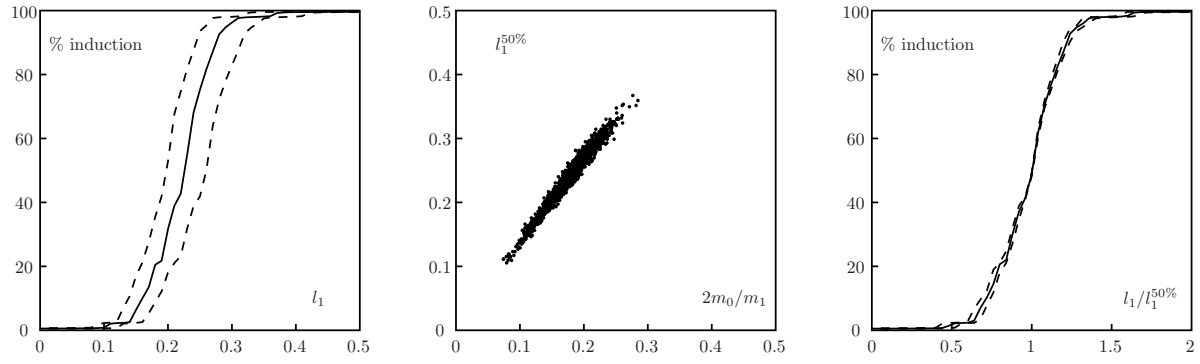

Figure S1: Induction of a single cell by EGF. The solid lines show the median and the dotted lines the lower/upper quartiles, indicating parameter uncertainty as determined by Monte Carlo sampling. (a) Average induction vs. absolute signal level. Experimental observations (Table S1, line 3) imply that induction is complete for $l_1 = .5$. (b) Scatter plot of the threshold $l_1^{50\%}$ for 50% induction vs. the theoretical value $2m_0/m_1$. (c) Induction vs. level relative to threshold. For each sampled parameter set, the $l_1^{50\%}$ value was computed and used to scale the l_1 dependence. Thus the uncertainty in the response is mostly on the threshold, and would be greatly reduced if measurements of signals levels were available.

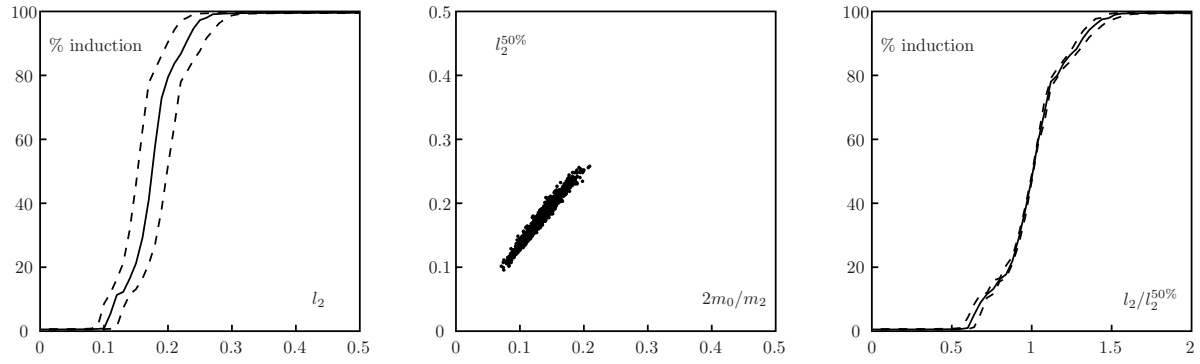

Figure S2: Induction of a single cell by Notch. As in Fig. S1, the solid lines show the median and the dotted lines the lower/upper quartiles. (a) Induction vs. absolute signal level. Experimental observations (Table S1, line 4) imply that induction is complete for $l_2 = .5$. (b) Threshold $l_2^{50\%}$ for 50% induction vs. the theoretical value $2m_0/m_2$. (c) Induction vs. level relative to threshold.

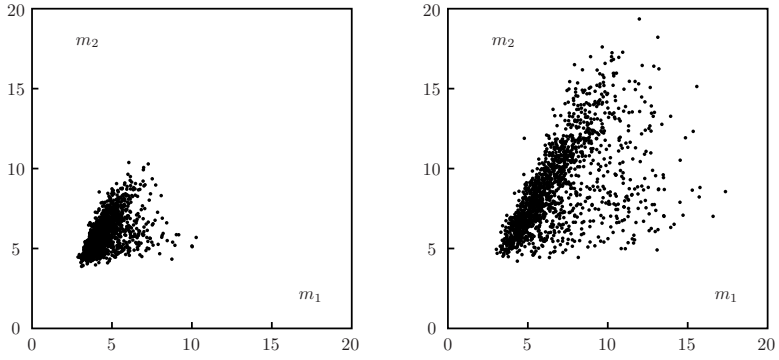

Figure S3: Scatter plots of the signal response strengths, m_2 vs. m_1. (a) With our default priors. (b) With relaxed priors (the standard deviation, β in Eq. S18, was increased from 4 to 16). Thus the data by itself does not strongly constrain the magnitude of the m_i. But extreme pathway sensitivities we consider improbable.

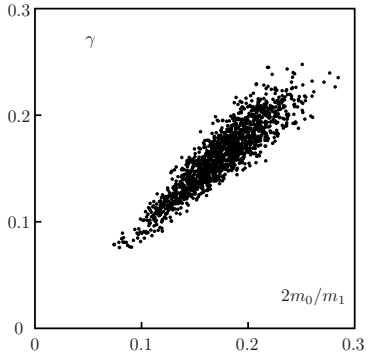

Figure S4: Scatter plot of γ vs. $2m_0/m_2$.

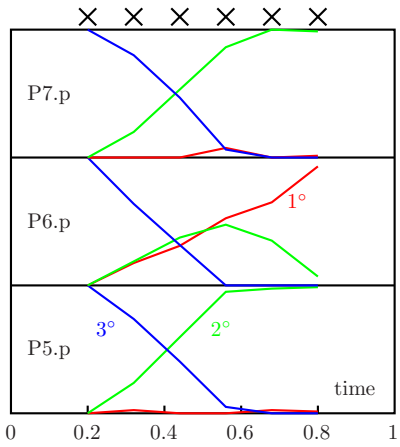

Figure S5: Experimental time courses for AC ablation, showing a gradual transition from no induction to the WT pattern (cf. Table S1, lines 9-14; [S15]). Fate proportions are plotted as a function of ablation time (developmental stages mapped to model times), with the colors indicating the three fates. Crosses denote ablation times as in Fig. 5B.

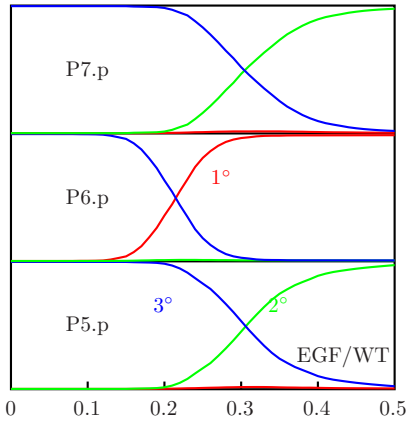

Figure S6: Predicted EGF hypomorph phenotypes. Fate proportions vs. EGF level (relative to WT). Note that a WT phenotype for 0.5 WT EGF is part of the data being fit (Table S1, line 3).

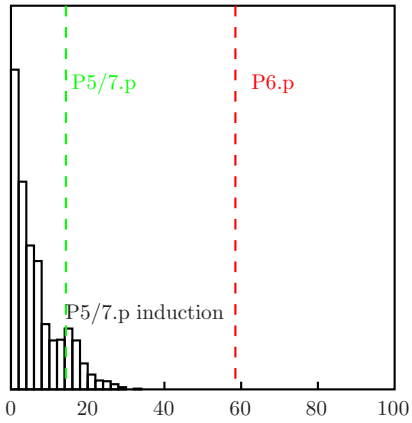

Figure S7: Predicted P5/7.p induction in an EGF hypomorph (*lin-3(e1417)*, Table S4). EGF level ($\approx .2$) is fit to match the level of P6.p induction (58%; dashed red line). Qualitatively, we correctly predict that P5/7.p induction is much less than P6.p induction, in contrast with the outcome following AC ablation (Fig. S5). Quantitatively, the experimental P5/7.p induction (15%; dotted green line) falls within the predicted distribution.

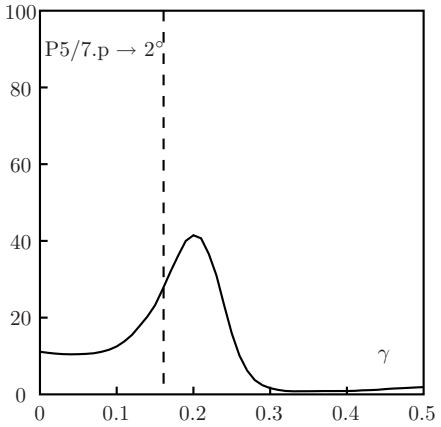

Figure S8: EGF contributes to robustness of 2° fate induction. The level of EGF seen by P5/7.p (γ) was varied in a background with reduced lateral signaling (WT/4). Maximum induction of P5/7.p to the 2° fate is obtained for an intermediate value of γ, which is of the same order as its mean value in our fit (dashed line).

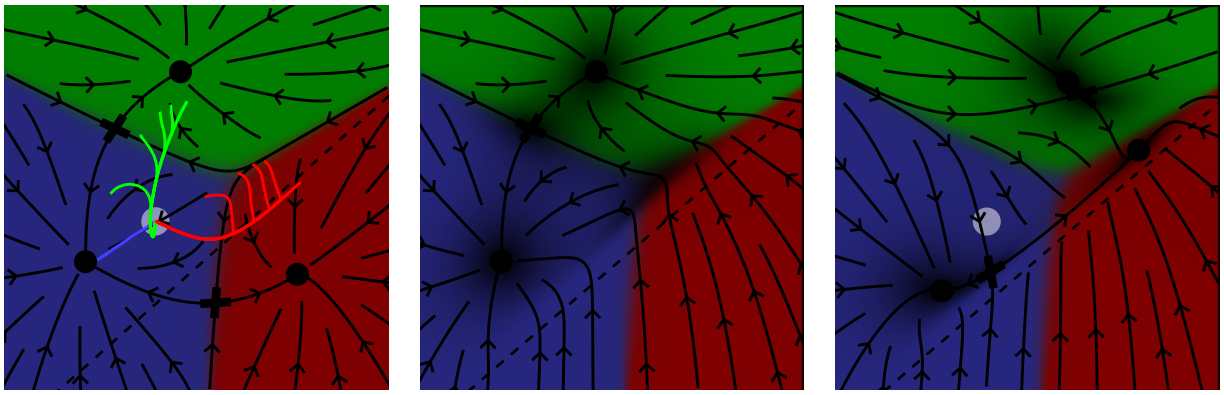

(a) AC ablation (b) Autocrine only (c) EGF(rf)

Figure S9: Geometric interpretation of phenotypes. (a) Average trajectories for AC ablations at successive times are overlaid, showing the progressive transition from no induction to a WT pattern. P6.p outcomes at intermediate times are located along the 1°/2° boundary, corresponding to the comparable proportions of 1°/2° fates observed experimentally (Fig. S5). (b) Flow seen by P6.p after AC ablation (EGF set to 0). The colors show as in (a) the basins of attraction in the absence of external signals, which define fates, but autocrine Notch signaling was included to compute the flow lines. The 1° fixed point then disappears, i.e. all induced cells would reach the 2° fate given sufficient time. However, when the magnitude of the flow is plotted (darker colors represent slower flow, e.g. near the fixed points), it becomes apparent that there is a region of slow flow near the 1°/2° boundary (the "shadow" of the 1° fixed point), where cells can remain for an extended time. The comparable proportions of 1°/2° fates adopted by P6.p at intermediate ablation times thus appear as a consequence of the geometry of the flow – rather than contingent on precise timing. (c) Flow seen by P6.p (autocrine signaling included; colors as in a,b) in the presence of weak inductive signaling (corresponding to the EGF hypomorph in Fig. 7B). The trajectories now converge onto a line connecting fixed points in the 1° and 3° domains (the outflow of the saddle between the two fates), explaining why P6.p yields no 2° fates in that case.

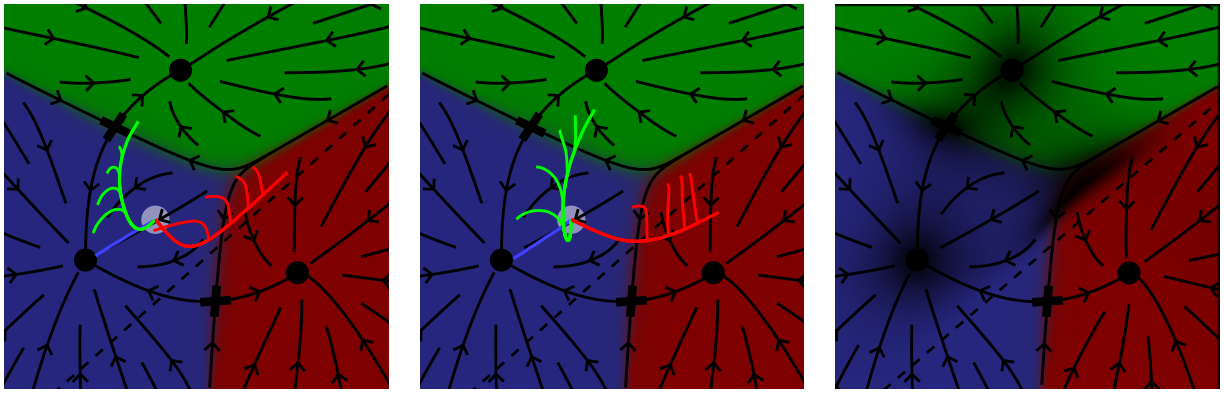

(a) EGF(rf) (b) Notch(rf) (c) Notch(rf)

Figure S10: Predicted ablation phenotypes in mutants. (a,b) Average trajectories for different ablation times are overlaid as in Fig. S9a. (a) Reduced inductive signaling (.35×WT) increases the time (before ablation) needed for a given level of induction but intermediate phenotypes exhibit comparable proportions of 1°/2° fates for P6.p (cells end on the boundary), as in WT. This is consistent with these mixed fates being a robust geometrical property of the flow (Fig. S9b) (b) In contrast, reduced lateral signaling (.5×WT – no phenotype in the absence of ablation) displaces P6.p outcomes into the 1° domain. (c) P6.p outcomes under reduced lateral signaling are explained by a shift of the region of slower flow (darker colors) where cells end (compare with Fig. S9b).

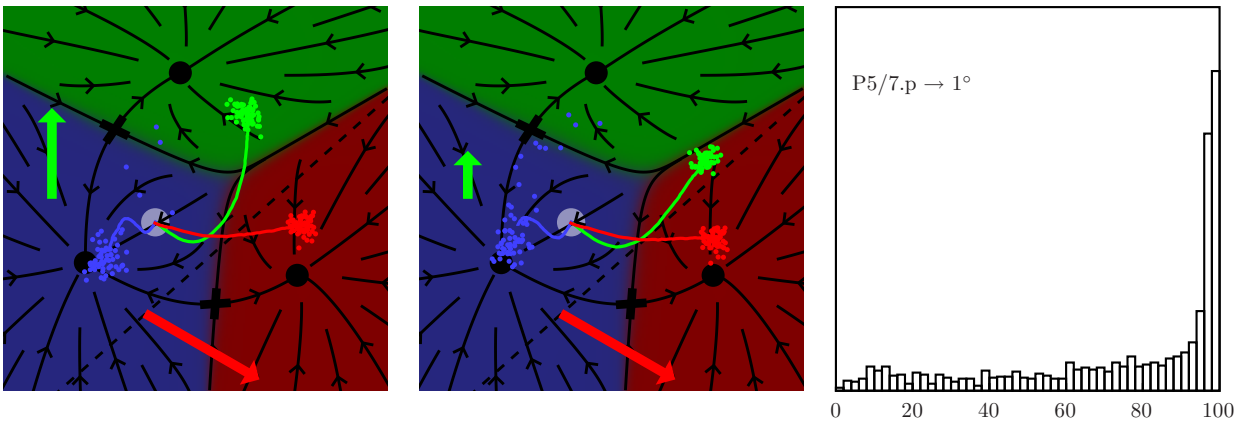

(a) EGF(gf) (b) EGF(gf);Notch(rf) (c) EGF(gf);Notch(rf)

Figure S11: Marginal crosses: EGF(gf)×Notch(rf). (a) A marginally WT increase in inductive signaling (≈ 4×WT) shifts P5/7.p near the boundary between the 2° and 1° domains. (b) When lateral signaling is reduced in this background (≈ .5×WT), inductive signaling prevails and P5/7.p are converted to 1° fates. (c) Distribution of P5/7.p induction to a 1° fate in the parameter ensemble, showing that a strong phenotype is likely.

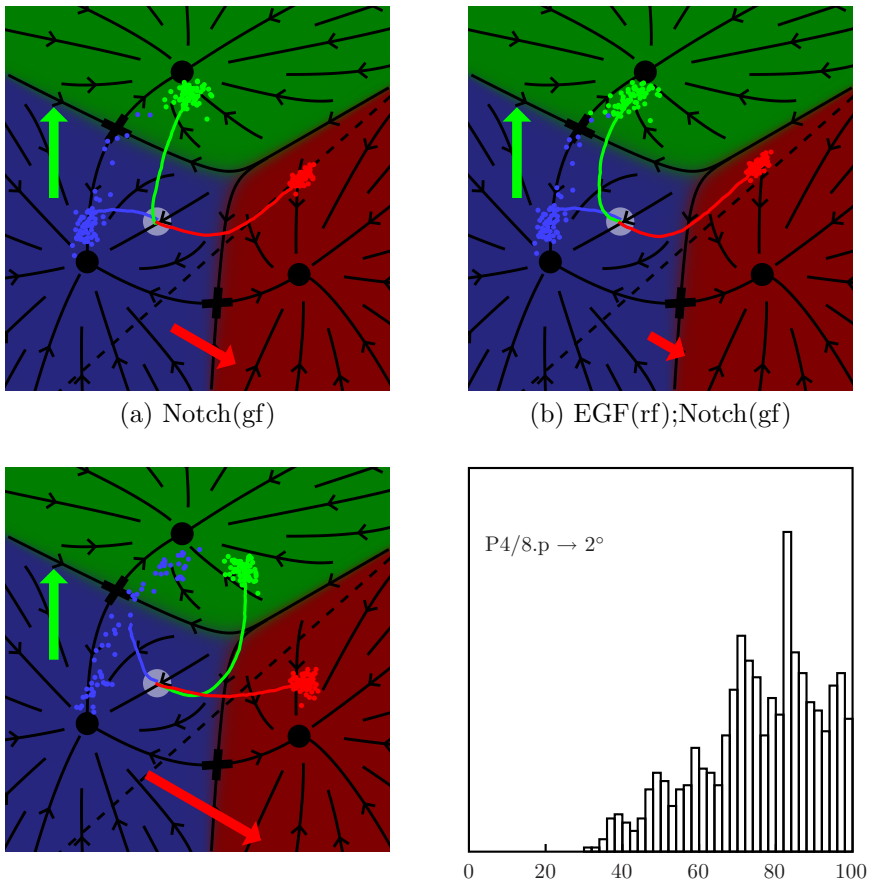

(a) Notch(gf)

(b) EGF(rf);Notch(gf)

(c) EGF(gf);Notch(gf)

(d) EGF(gf);Notch(gf)

Figure S12: Marginal crosses: EGF(gf)×Notch(gf). (a) A marginal level of constitutive Notch activity (≈ .1) shifts P4/8.p (normally 3°, in blue) near the boundary of the 2° domain. (b) A WT phenotype is still obtained if this is combined with a silent reduction in inductive signaling (≈ .5×WT). (c) When inductive signaling is instead increased (≈ 4×WT) P5/7.p come closer to the 1° fate, resulting in enhanced lateral signaling early in their trajectory, and P4/8.p can be converted to the 2° fate. (d) Distribution of P4/8.p induction to a 2° fate in the parameter ensemble, showing that this is a robust prediction.

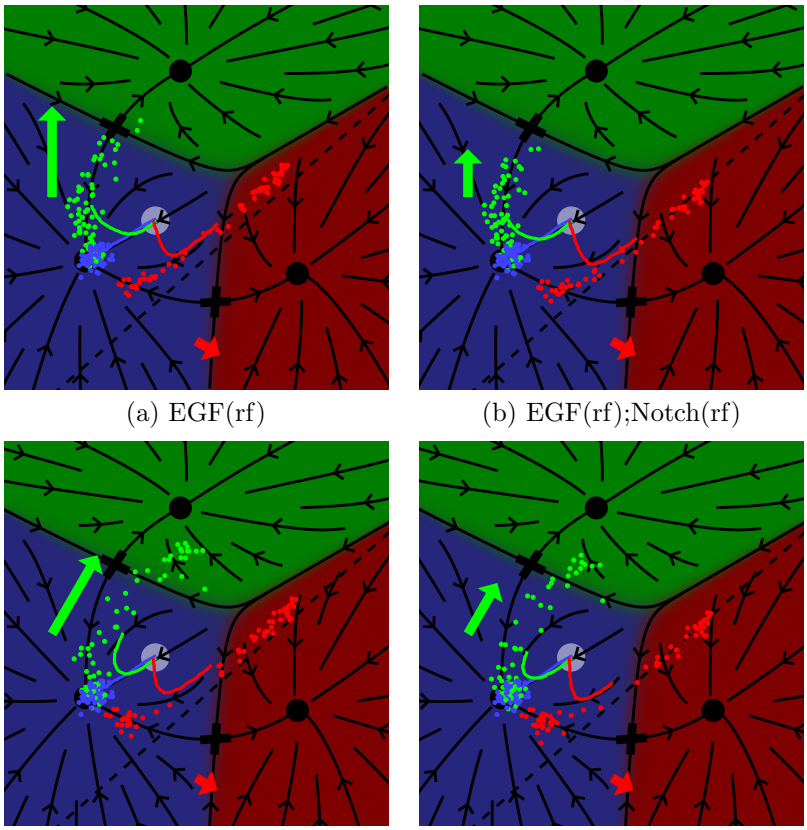

(a) EGF(rf) (b) EGF(rf);Notch(rf)

(c) EGF(rf) (d) EGF(rf);Notch(rf)

Figure S13: Cross between an EGF hypomorph (*lin-3(e1417)*, Table S4) and a marginal Notch hypomorph. (a,c) show the EGF hypomorph and (b,d) the cross. With the canonical directions of the vectors $\vec{m}_i$ representing the pathways (a,b), a marginal reduction of lateral signaling has little effect on P6.p induction in an EGF hypomorph. With $\vec{m}_2$ rotated clockwise (c,d), P6.p induction is reduced in the double mutant (from 58 to 45%).

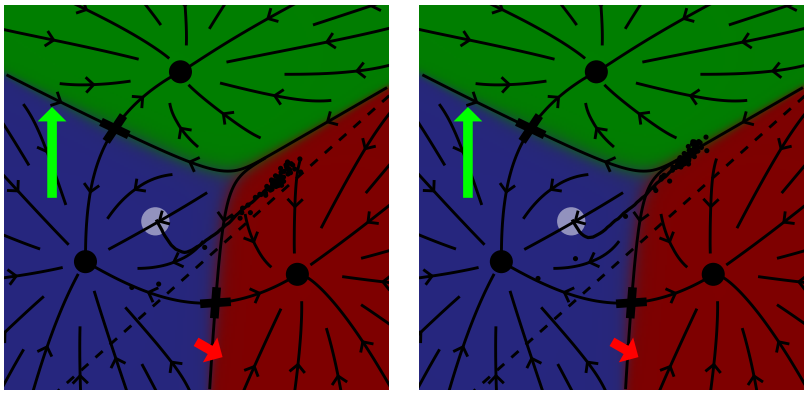

(a) (b)

Figure S14: Isolated cell fates. (a) If diffusing lateral signal is mostly lost to degradation, an isolated cell at intermediate levels of EGF is equivalent to P6.p in a hypomorph (Fig. 7) and cannot adopt a 2° fate. (b) If on the other hand adjacent cells compete for diffusing lateral signal then an isolated cell can receive much more of the signal it secretes than if it had neighbors. Here, with EGF = .275 WT and a 5-fold increase in autocrine signaling we obtain isolated 2° cells at a frequency close to experiment. If we model the separate fates of VPC daughters, we recover the observed high frequency of hybrid 1°/2° fates (Table S7).

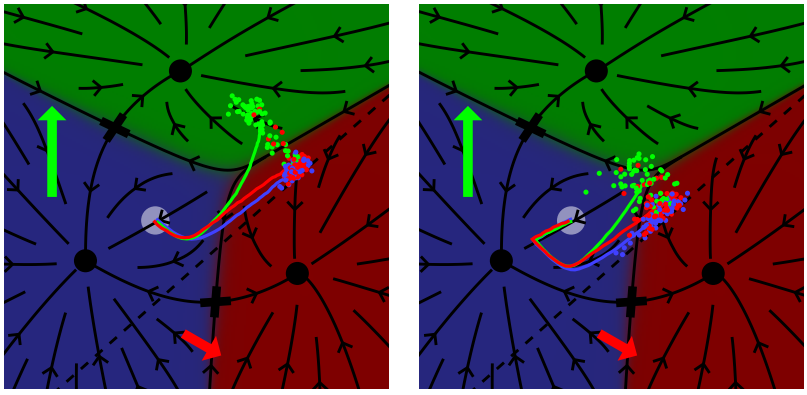

(a) (b)

Figure S15: Timed induction uncovers intermediate fates. (a) A uniform level inductive of inductive signal ($l_1 = 0.5$) yields the predominant pattern 12121, and we predict that P5/7.p travel through the 1° domain on their way to the 2° fate – before lateral signaling sets in. (b) These intermediate states could be revealed by delaying induction – leaving less time for lateral signaling to drive P5/7.p to the 2° fate. Here, l_1 was set to 0 until $t = 0.4$ then to 0.5 as in (a). This prediction could be tested using a temperature-sensitive allele of *lin-15*.